Flow Measurement and Instrumentation 44 (2015) 97–106

Contents lists available at ScienceDirect

Flow Measurement and Instrumentation

journal homepage: www.elsevier.com/locate/flowmeasinst

Flow structure in critical flow Venturi nozzle and its effect on the flow rate

E. von Lavante [a,*], H. Kaya [a], F. Winzösch [a], S. Brinkhorst [a], B. Mickan [b]

[a] University of Duisburg-Essen, Faculty of Engineering, Lotharstr. 1-21, D 47057 Duisburg, Germany
[b] Physikalisch-Technische Bundesanstalt, Braunschweig, Germany

ARTICLE INFO

Available online 23 December 2014

Keywords:
Critical flow Venturi nozzle
Shock structure
Unsteady flow
Discharge coefficient
Unchoking

ABSTRACT

The flow fields in toroidal Venturi-nozzles, shaped according to the ISO-9300 Standard, have been investigated using numerical flow simulation. The present study was aimed at clarifying some of the phenomena associated with unchoking the flow in the throat. To this end, the shock structure has been studied for different Reynolds numbers and exit pressure ratios. The flow simulations were carried out in two and three dimensions. The flow fields were always unsteady, displaying a complex shock–boundary layer interaction.

1. Introduction

One of the simplest methods of highly accurate measurement of mass flows as well as volumetric flow rates at normalized conditions is the employment of critical nozzles. The guidelines and standards in using these devices are well defined and covered by the ISO-9300 Standard [1]. Its validity range is limited to Reynolds numbers between 10^5 and 10^7. However, even within these limits, at the lower part of the range several investigators [2–4] have discovered flow effects that were not consistent with the simple quasi-one-dimensional theory. These included variation of the discharge coefficient C_D as a function of the nozzle back pressure not explainable by the theory offered in ISO 9300 [1], occurrence of instabilities and pressure waves traveling upstream all the way through the throat and thus unchoking the nozzle for a very brief period of time, and the so called premature unchoking. After calibration, the corresponding nozzles still offer the same very reliable means of gas metering, however, as long as they are employed within their specifications. The flow fields in nozzles with Reynolds numbers below the range given by the standard ($Re = 1.0 \times 10^3$–4.4×10^4) have been investigated by von Lavante et al. [5] experimentally as well as numerically.

More recently, Nakao and Takamoto [6] and Nakao [7] presented extensive studies of the choking phenomenon aimed at shedding more light on this problem. The flow in a model nozzle has been simulated in two dimensions and compared to the corresponding experimental work in [8]. Generally, the comparison between experimental data and numerical results given in [8] is poor. As this work is related to the subject of the present work, it will be discussed in more detail below. Finally, Mickan et al. [9] not only presented a plethora of experimental results related to the choking/unchoking phenomena, but also offer a plausible theory aimed at explaining some of their aspects. Instead of using the somewhat ambiguous expression “premature unchoking” they suggest the more descriptive expressions “low unchoking” and “high unchoking”, which the present authors will also employ.

The aim of the present work was to investigate the flow behavior in sonic nozzles in general, and the choking phenomenon in particular. To this end, the present authors have carried out several numerical flow simulations of one critical flow Venturi nozzle (CFVN) geometry in two and three dimensions. The Reynolds number was at this time fixed at $Re_D = 140{,}000$; however, the exit pressure ratio was varied between 0.2 and 0.8. The present investigators used the program ACHIEVE developed by the first author as well as the commercial code CD-adapco Star CCM+(CCM+).

2. Numerical methods

As the flow in the CFVN is always unsteady (if in doubt about this point, the interested reader is invited to listen to the CFVN operating —the noise is a clear indication of the unsteadiness), compressible and viscous, a corresponding solver had to be selected for the present work. In addition, the flow could be either laminar or turbulent, or both, depending on the Reynolds number. The geometry of the nozzle has been assumed to follow the ISO-9300 Standard. Initially, the flow was assumed to be two-dimensional axisymmetric, but later, fully three-dimensional flow field configurations were investigated. It will be shown below that the flow in the nozzle was in significant portions of the diffuser of three-dimensional character.

* Corresponding author.
E-mail address: ernst3.vonlavante@uni-due.de (E. von Lavante).

http://dx.doi.org/10.1016/j.flowmeasinst.2014.12.003
0955-5986/

The unsteady compressible viscous flow in the nozzles was therefore simulated using the Navier–Stokes solver ACHIEVE, developed by the first author. The code is based on Roe's Flux Difference Splitting in finite volume form employing a special quadratic van Albada limiter in order to minimize the numerical dissipation. The details of this code can be obtained from, for example, von Lavante and Grönner [10]. Traditionally, this code was by far superior to any commercial program in being able to resolve the complex flow structure in the CFVN. However, the recent version of the commercial program CCM+ proved to be able to give results that were comparable to those of ACHIEVE, providing an easy to use option to ACHIEVE. The coupled solver (compressible flow solver) is equally based on Roe's averaging, which explains its quality of results, although the details of this code are not publicly available.

Computational grids of good quality were essential for obtaining any results; here, the local resolution, grid stretching and cell skewness were important. The present grids consisted of between 17,600 cells (coarse) and 122,160 cells (fine) arranged in 3 to 4 blocks in two dimensions and approximately 5.5 M cells in 4 blocks in three dimensions.

All of the present computations were carried out for the same geometry and inflow conditions. Here, a Venturi-nozzle according to ISO 9300 was taken, with a diffuser half-angle of 4°, diffuser length of 7 D^* (diameter at the throat) and $D^*=9.89$ mm. The working fluid was air given at the inflow at $P_{00}=0.101325$ MPa and $T_{00}=300$ K.

Equally important are proper boundary conditions. The solver ACHIEVE is provided with genuinely non-reflective inflow and outflow boundary conditions. In CCM+, the non-reflective boundary conditions work only with steady flow; therefore, the outflow region had to be designed as a "dump" of pressure waves with ever increasing grid spacing for effective damping. Details of the boundary condition formulation in ACHIEVE can be found in, for example, Yao [11].

3. Two-dimensional results

3.1. Normal shock in outflow

In [9], it was shown that the mass flow in CFVNs displays in many cases a lower value than critical at relatively low outflow pressure ratio p_{out}/P_{00} (ratio of static pressure at the end of the diffuser to the inflow total pressure), called in [9] "low unchoking". It appeared at approximately $p_{out}/P_{00}=0.3$–0.6, which corresponds to a flow condition at which, theoretically, a normal shock forms just at the exit from the diffuser. In the present case, the theoretical outflow pressure ratio, according to a simple quasi-one-dimensional theory, was 0.31. For comparison, a pressure ratio $p_{out}/P_{00}=0.2$ for smooth outflow was also simulated.

The simulations were performed by both ACHIEVE and CCM+.

At $p_{out}/P_{00}=0.31$, a normal shock formed indeed in the diffuser; it was, however, always unsteady, forming inside the diffuser and moving to the outflow location and, after bypassing it, further downstream. Eventually, it dissipated to a pressure wave that was passed out of the computational domain. Upstream of the exit shock, a complex lambda–shock–boundary layer interaction with massive unsteady flow separation was present, with the lambda–shock moving upstream and the normal exit shock moving downstream.

In Fig. 1, a normal shock moving downstream as well as two lambda–shocks moving upstream can be viewed. Clearly visible is also massive separation induced already by the first leg of the first shock. A detailed view of the first lambda shock at an earlier time (the shock being downstream of its location in Fig. 1) can be seen in Fig. 2. Here, the stream lines are shown as well, making the determination of the deflection angle and the wave angle possible. The deflection was measured as $\delta=9°$ and the wave angle $\beta=34°$. The Mach number ahead of the normal shock at the center line was $M_x=1.9$, the one after the shock $M_y=0.50$. The later value was

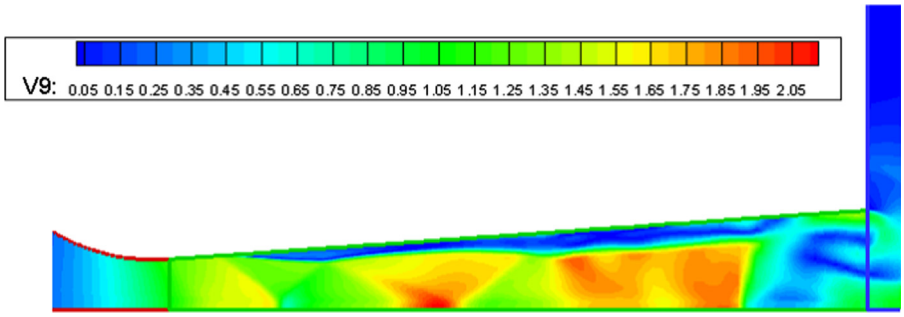

Fig. 1. Mach number contours, $p_{out}/P_{00}=0.31$.

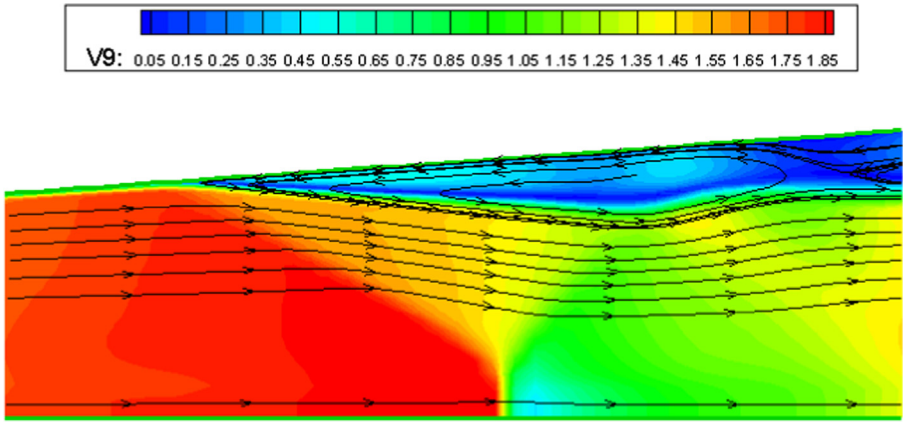

Fig. 2. Detail of the first lambda shock.

somewhat low, but it should be recollected that the shock is moving in upstream direction.

The above values can be compared to the theoretical results given by the quasi-one-dimensional theory, to be found in, for example, NACA report 1135 [12]. It is important, however, to notice that the conical solution of the oblique shock relationships has to be taken. Fig. 3, taken from the NACA 1135 [12], shows the difference between the two-dimensional wedge-type shock and the conical shock solution.

The present results, given by the program ACHIEVE, agree fairly well with the present three-dimensional results, given in the following chapter below.

As the total pressure is a direct indication of the losses and closely coupled to the value of entropy, it should be considered presently. In Fig. 4, the total pressure ratio P_t/P_{00}, where P_t was the local value of the total pressure and P_{00} was the total pressure at the inlet, is displayed for the flow field in Fig. 1. As expected, the pressure ratio P_t/P_{00} remains below one (Fig. 6).

At a later time, the normal shock passes the exit and moves through the free jet downstream of the diffuser, forming a Mach-disk. In the diffuser, the first lambda shock moved all the way upstream, and downstream of the second lambda shock, a new normal shock is forming. Although moving in the positive flow direction, it is fairly strong as the Mach number ahead of it was in excess of 2.35.

Again, a large separated zone at the upper boundary is noticeable. The corresponding plot of total pressure ratio bears some surprises.

The total pressure increases across the shocks!! This seeming violation of the second law of thermodynamics was first puzzling, more so as most of the classical lectures on gas dynamics do not mention this effect. The first indication that an increasing total pressure across moving shocks is possible was found in an unassuming but highly practical book by Zucker [13]. Consequently, the present authors undertook a little study of the total pressure ratio development as a function of the Mach number ahead of a moving shock M_1 and the Mach number of the shock movement M_S. Taking first the total pressures relative to the moving shock (relative system), no unexpected results were obtained, Fig. 7. The ratio P_t/P_{00} remains below 1.0 and approaches 1.0 as the Mach number M_1 is approaching 1.0 as well.

Taking, however, the total pressure ratio P_t/P_{00} in the absolute reference frame, relative to the stationary observer, a totally different picture is obtained, see Fig. 8.

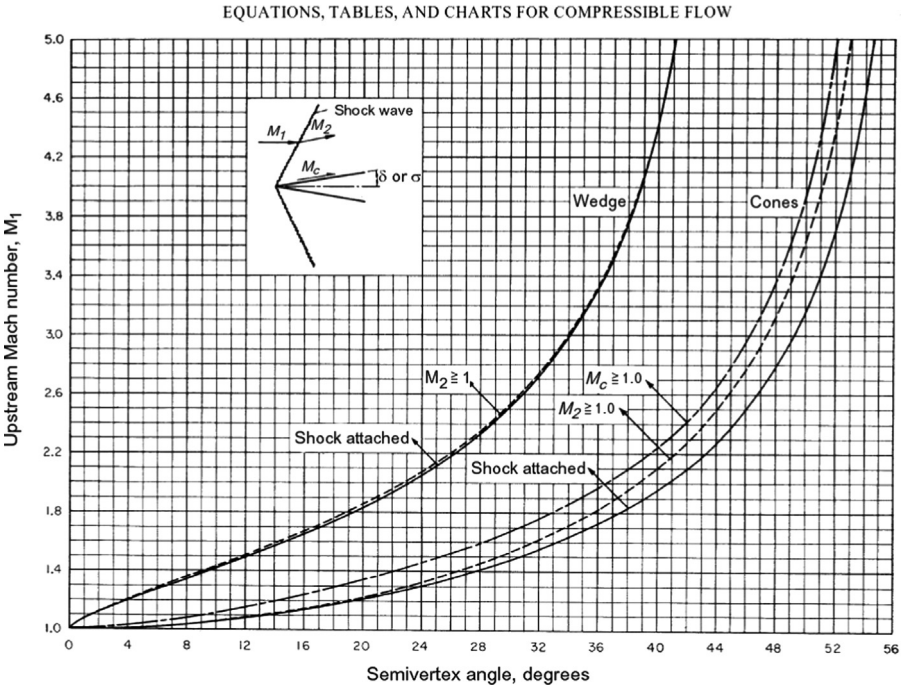

Fig. 3. Comparison of oblique shock results between two-dimensional shock and conical shock, from [12].

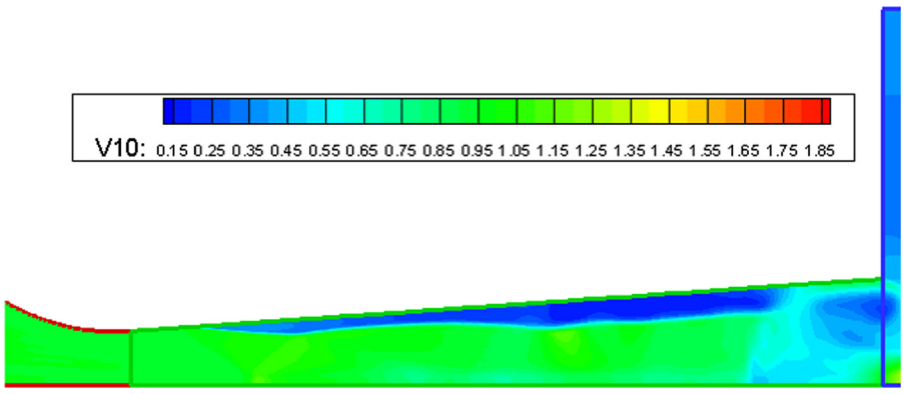

Fig. 4. Total pressure ratio P_t/P_{00} for the flow field in Fig. 1.

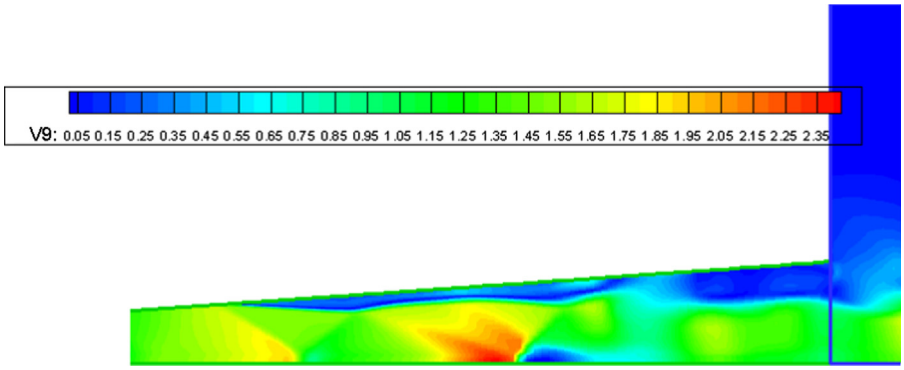

Fig. 5. Mach number contours, $p_{out}/P_{00}=0.31$.

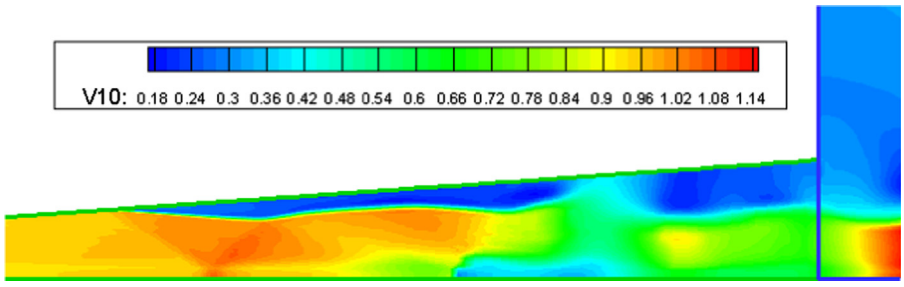

Fig. 6. Total pressure ratio P_t/P_{00} for the flow field in Fig. 5.

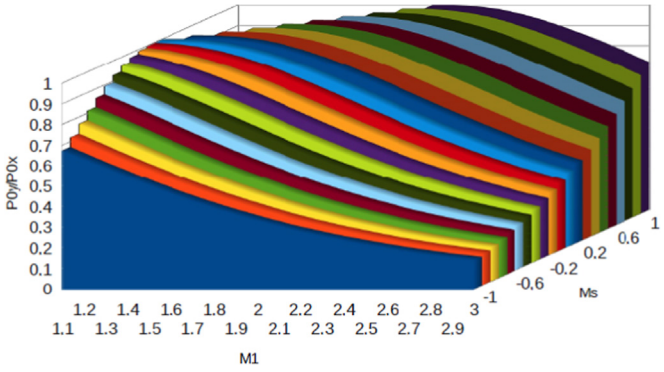

Fig. 7. Total pressure ratio P_{0x}/P_{0y} relative to the moving shock.

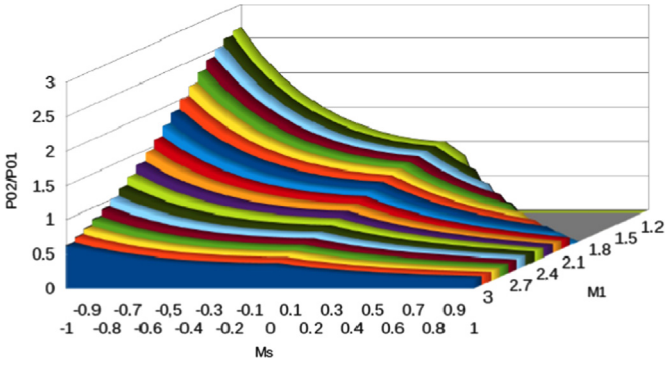

Fig. 8. Total pressure ratio P_t/P_{00} relative to a stationary observer.

Total pressure ratios in the case of negative shock Mach numbers (as present in Fig. 5) reach well over 1.0. Clearly visible is also a ridge of values close to 1.0 extending diagonally across the diagram, marking the situation where the relative Mach number ahead of the shock is nearly 1.0.

4. Mass flow as a function of outflow pressure ratio

In the next study, aimed at supplementing and, if possible, providing further explanation to the theoretical frame work postulated in [9], the flow in the same nozzle as employed in the previous chapter was studied for different pressure ratios at the outflow from the diffuser, p_{out}/P_{00}. Again, the Reynolds number was $Re_D=140{,}000$, implying that the flow in the nozzle was predominantly laminar. As the low unchoking was expected at pressure ratios p_{out}/P_{00} between 0.3 and 0.6, the present work included following pressure ratios p_{out}/P_{00}: 0.20, 0.25, 0.30, 0.35, 0.40, 0.50, 0.60 and 0.70. In this study, only the commercial code CCM+ was used, as it proved to be capable of delivering results of similar quality as those obtained by ACHIEVE. The resulting mass flow can be seen in Fig. 9.

Mass flow through the nozzle throat, as obtained from spatial and time-wise integration at the throat, indicated low unchoking at a pressure ratio of approximately $p_{out}/P_{00}=0.40$, similar to the experimental data described in [9]. For all the pressure ratios, the flow was unsteady, with shocks moving within the diffuser and beyond. One should expect these results in the view of the massive separation caused by the shocks. Extensive separation like the one shown in Fig. 2, for example, will be neither steady nor symmetric. The flow field in the case of $p_{out}/P_{00}=0.2$ can be considered in Fig. 10.

The flow field displays no strong, almost normal, shocks; the oblique shocks were moving within the containment of the diffuser and never reached the throat. Consequently, the mass flow rate was constant at a value close to the rate given by the ISO-9300 Standard. The corresponding plot of the wall shear stress (blue, left scale) and entropy (red, right scale) at the wall is given in Fig. 11. It is interesting to note that, as expected, the wall shear stress reaches its maximum in the throat, and its minimum in the separated region. The entropy increases all the way to the first leg

of the lambda shock, then increases sharply in the shock and falls off after the shock. The steep decrease is at first difficult to grasp; however, Fig. 2 helps to explain this phenomenon. Specific entropy is an intensive property, transported by particles along streamlines. In the case of separated flow in Fig. 2, the streamlines originated all the way downstream in the low Mach number region above the free jet, in the "reservoir" of low entropy fluid, transporting it upstream through the separated boundary layer.

The flow field in one instant of time for the ratio $p_{out}/P_{00}=0.35$ is shown in Fig. 12. As in the simulations performed by ACHIEVE, a system of two lambda shocks followed by an almost normal shock can be observed.

The corresponding plot of the wall shear stress and entropy are displayed in Fig. 13.

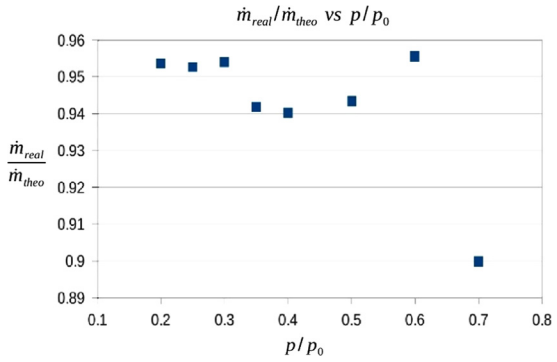

Fig. 9. Computed mass flow ratio through the nozzle throat as a function of p_{out}/P_{00}.

As already stressed above, it was found that the flow fields were in all cases unsteady. However, as long as the unsteady movement of the shock systems was limited to the diffuser and did not reach the throat, the mass flow was approximately constant, corresponding to the choked condition. Even in this case, the pressure fluctuations could propagate from the diffuser upstream through the boundary layer, resulting in small changes of the mass flow—an effect observed also experimentally. The low and high unchoking was the result of the shock system, changing from lambda–shock to weak normal shock, moving in upstream direction throughout the throat. The shock movement is the result of complex interaction of the shock system with the boundary layer, being mainly affected by the always present separation. In addition, it is expected that for cases with the Reynolds number Re_D close to 10^6 (the limiting value at which the transition from laminar to turbulent takes place in the throat or upstream of it) the shock–boundary layer interaction will also initiate transition, complicating matters even more. More on this subject can be found below in Section 6.

5. Three-dimensional results

In view of the massive unsteady boundary layer separation, the flow field will most likely fail to remain axisymmetric due to stochastic fluctuations within the separated region. Besides, several investigators have experimentally found asymmetric shock systems even in symmetric geometries. Therefore, it is expected that the real flow in the CFVNs will be most certainly of three-dimensional character. The present authors realized this fact and accounted for it by carrying out a three-dimensional flow simulation within the same nozzle as used in the previous two studies.

At the present time, the commercial solver adapco Star CCM+ was rendered sufficient for this numerical work. The grid, consisting

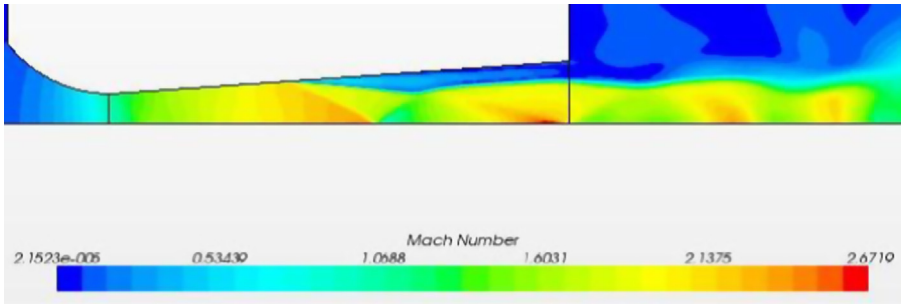

Fig. 10. Mach number contours, $p_{out}/P_{00}=0.2$.

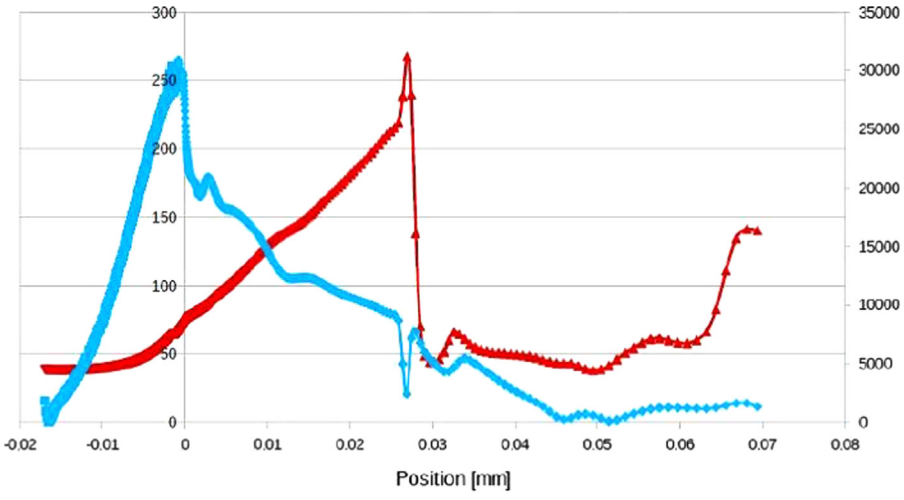

Fig. 11. Wall shear stress and entropy at the wall for flow given in Fig. 12. (For interpretation of the references to color in this figure, the reader is referred to the web version of this article.)

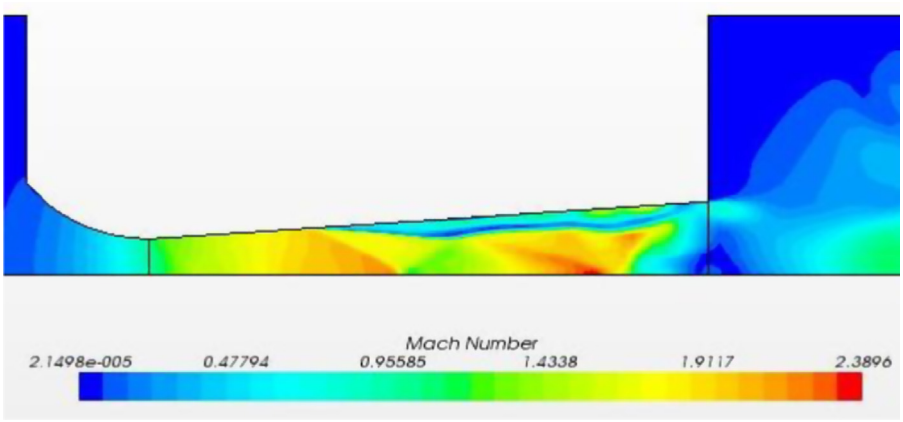

Fig. 12. Mach number contours, $p_{out}/P_{00}=0.35$.

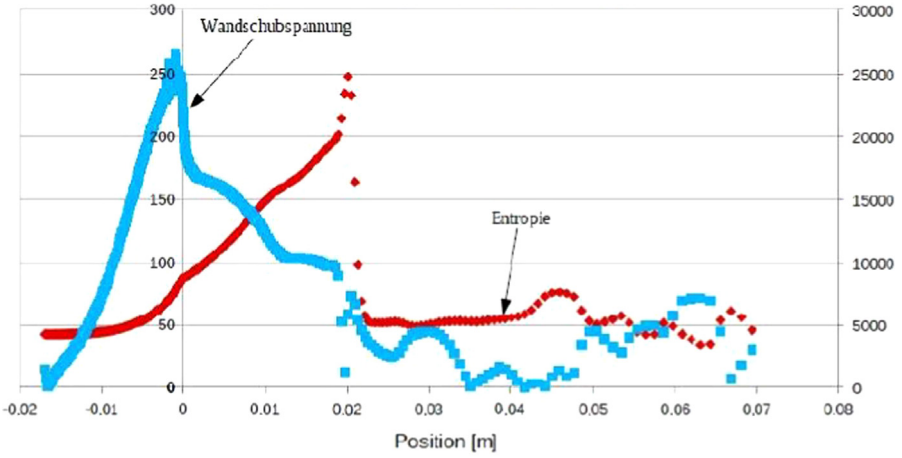

Fig. 13. Wall shear stress and entropy at the wall for flow given in Fig. 13.

of 5.5 M cells arranged in 3 blocks, was generated using the commercial program GRIDGEN. No turbulent model was implemented as the Reynolds number was relatively low at $Re_D=140{,}000$ and $Re_D=500{,}000$, implying mostly laminar flow. The outflow pressure ratios imposed on the diffuser were $p_{out}/P_{00}=0.7$–0.2, see Fig. 16.

As in all the two-dimensional simulations, the flow was unsteady for all three pressure ratios. The flow fields in the x–y plane along the geometric symmetry line are presented in Fig. 14 for comparison as Mach number contours. Again, a shock structure consisting of at least two lamba–shocks and possibly a terminating normal shock can be seen. As in the two-dimensional case, the first lambda shock induces boundary layer separation.

As can be seen in Fig. 14, the wave angle of the first lambda shock is decreasing with decreasing outflow pressure. The deflection angles were $\delta=9^\circ$, 8° and 6°, agreeing well with the theory of conical shocks. The shock itself is moving downstream with decreasing outflow pressure. The separated boundary layer after the first shock is unsteady; the amplitude of the fluctuations is growing as the diffuser exit is approached. It was observed that the separated layer was moving randomly in all three directions, thus creating rather complex flow field as it is interacting with the shocks in the core flow. In Fig. 15, four cross-sectional planes starting from the throat and moving downstream are shown. In the throat, the flow field was, within given numerical accuracy, axisymmetric. However, as the flow separated, it assumed, as expected, stochastic behavior. A detailed view of the cross-sectional movement of the separated flow is presented in Fig. 16. Although a proper analysis of the scales and the frequency spectrum of the eddies in Fig. 16 has not been performed, it was assumed that the resulting flow can be considered "very large eddy simulation".

A fully three-dimensional view of the flow is offered in Fig. 17.

The corresponding mass flow in terms of the non-dimensional discharge coefficient C_D can be seen in Fig. 18, as compared to the equivalent mass flow obtained from two-dimensional flow simulation. Although qualitative agreement might be deduced with some phantasy, the amplitude of the mass flow decrease at low unchoking is much smaller in the three-dimensional case than in the two-dimensional result.

In view of the present results, as seen in Figs. 14–18, one has to express severe reservations about the realistic character of any two-dimensional flow simulation in CFVNs.

The C_D coefficient plot as a function of the outflow pressure ratio for a higher Reynolds number, $Re_D=500{,}000$, can be seen in Fig. 19. The amplitudes of the mass flow decrease as well as the qualitative character of the plot are very similar to Fig. 18; however, the position of the "low unchoking" is shifted toward higher pressure ratio p_{out}/P_{00}.

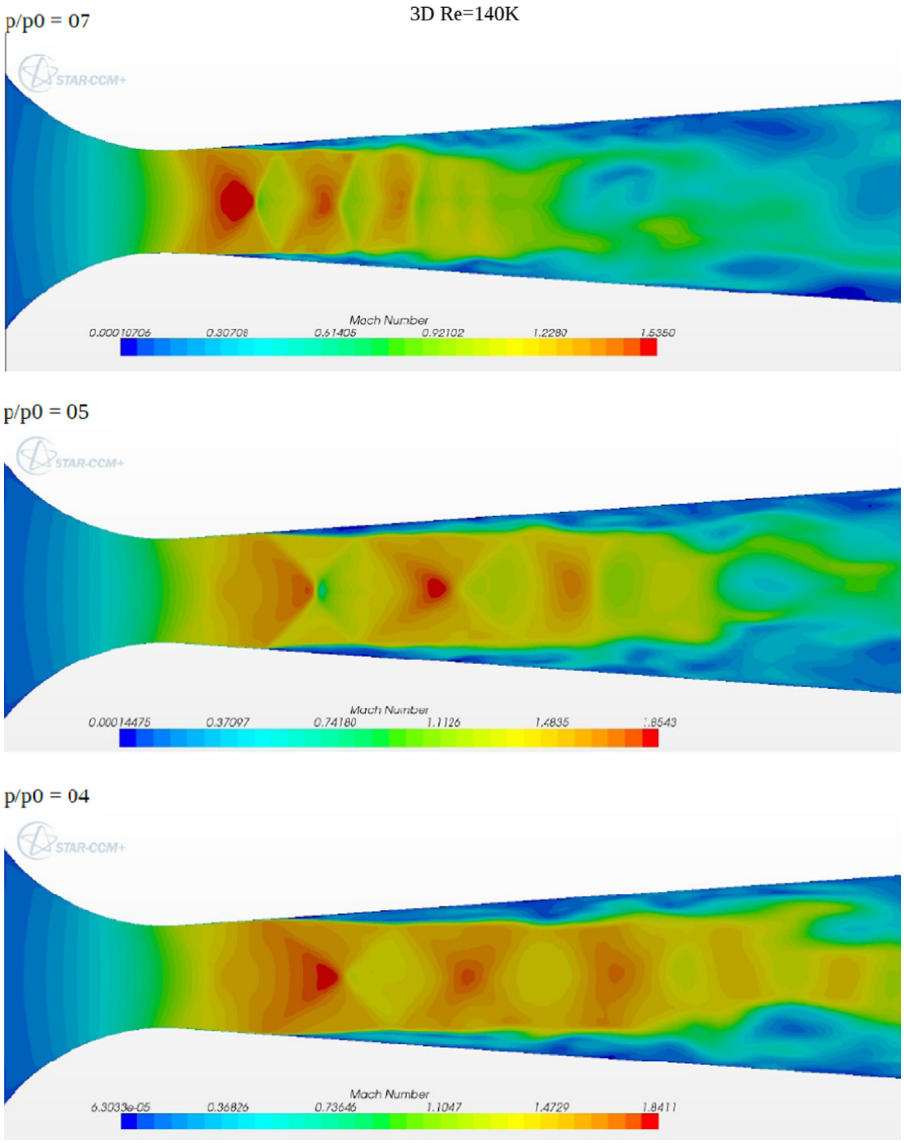

Fig. 14. Mach number contours for the three-dimensional results along a symmetry-plane for three different pressure ratios p_{out}/P_{00}=0.7, 0.5 and 0.4, Re_D=140,000.

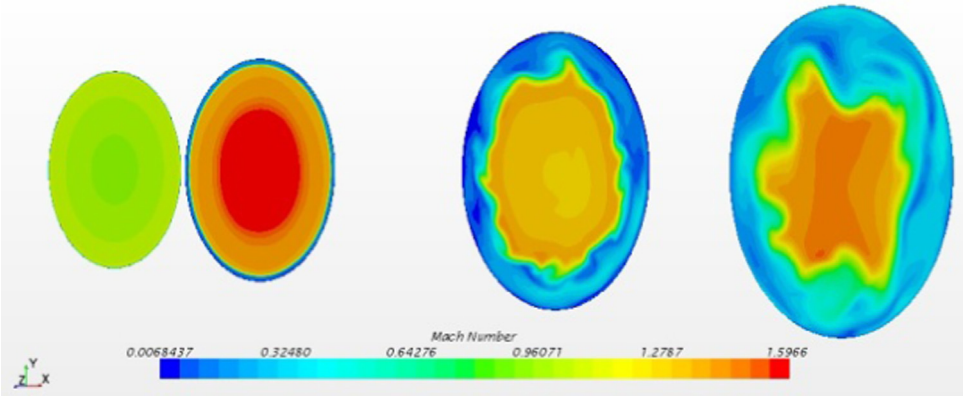

Fig. 15. Mach number contours in four cross-sectional planes.

6. Discussion of the results

The present results must be considered in view of the more recent findings by other investigators. In view of the difference between the two-dimensional and three-dimensional results, and the extremely complex flow field in three dimensions, it is difficult to make a clear statement regarding the relatively simple theory put forward in [9]. As any two-dimensional wedge-type nozzle always includes corner flow, this configuration is totally different from the axisymmetric CFVNs used in flow metering, being of

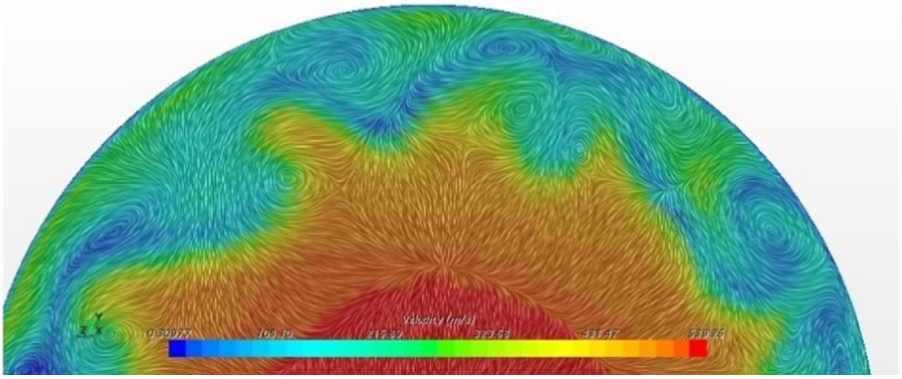

Fig. 16. View of vortical structure at the exit from the diffuser, $Re_D = 140{,}000$.

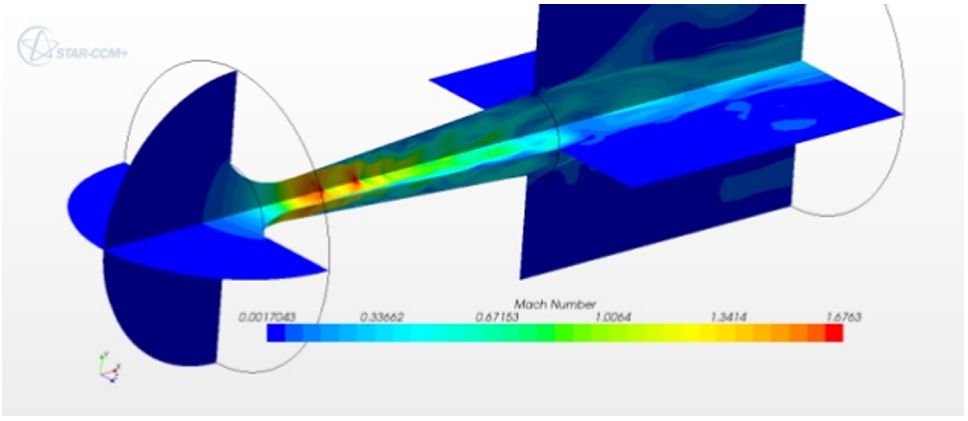

Fig. 17. Three-dimensional view of the Mach contours, $p_{out}/P_{00} = 0.7$, $Re_D = 140{,}000$.

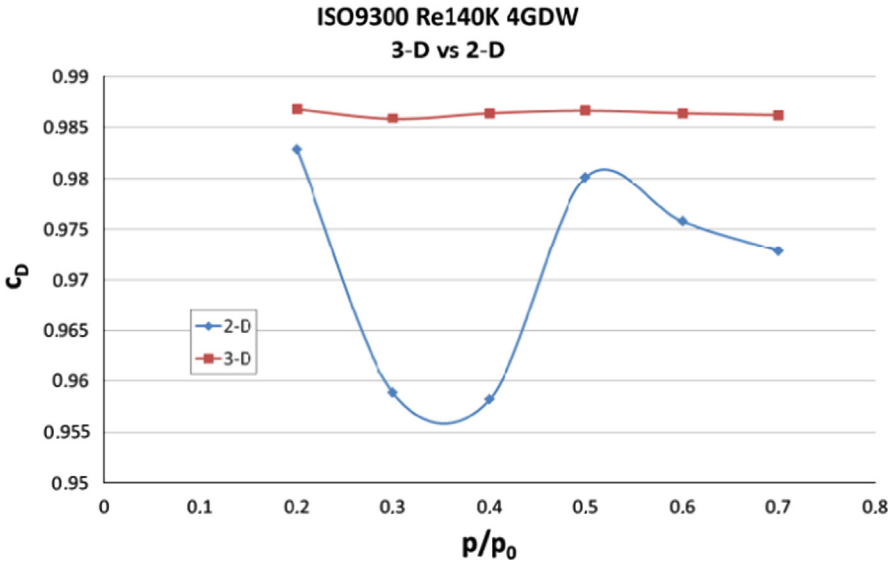

Fig. 18. C_D—coefficient, comparison between two-dimensional and three-dimensional computations, $Re_D = 140{,}000$.

hardly any significance. The numerical simulations in [8] were unsuited for the purpose stated; the two-dimensional assumption is not valid even on the symmetry line and the turbulence model (k–ω) way too dissipative for the present application. The authors of [8] admit that the numerical results were steady despite the experimental data indicating unsteady flow.

Much better basis for further theoretical considerations is the work by Deck et al. [14], published 5 years prior to [8]. Here, both a two-dimensional and a three-dimensional axisymmetric nozzles have been studied. The numerical flow simulations included two-dimensional simulations, three-dimensional simulations in the two-dimensional geometry and three-dimensional simulations in the "real" axisymmetric nozzle. The shadow-graph of the lambda–shock in the two-dimensional nozzle obtained by [14] can be seen in Fig. 20.

In all three pictures, the instability is induced by the first leg of the lambda shock, as expected. It is triggering large scale turbulence; however, its character could be described only after proper

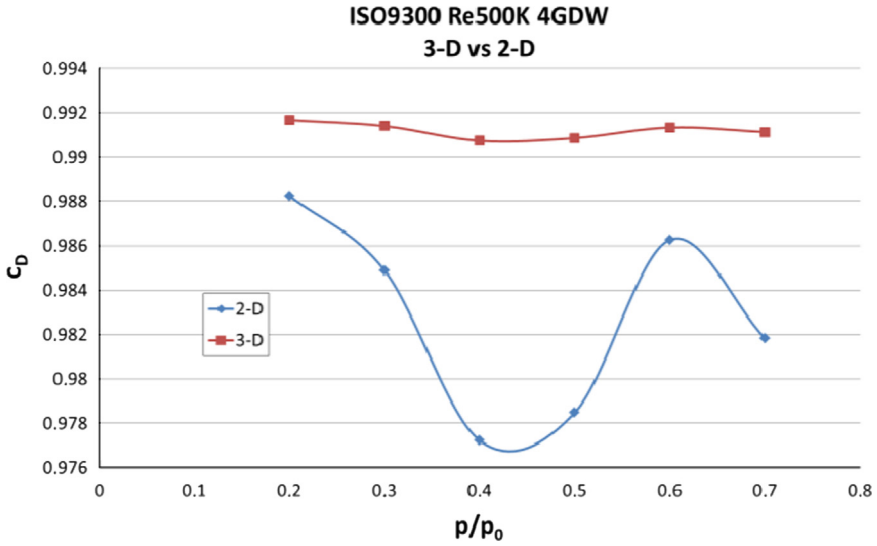

Fig. 19. C_D—coefficient, comparison between two-dimensional and three-dimensional computations, Re_D=500,000.

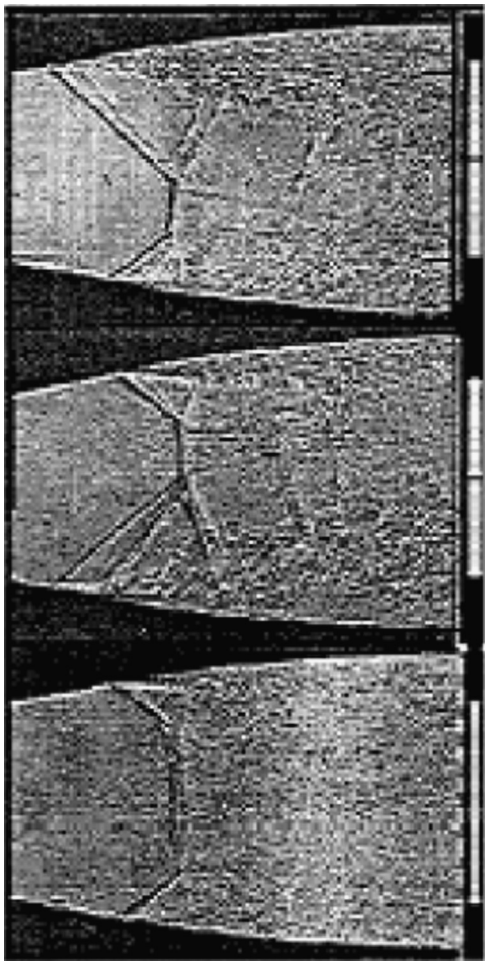

Fig. 20. Shadow graph of the lambda shock in two-dimensional nozzle, from [14].

analysis of the scales of the structures and the spectrum within the layer. The second leg of the lamba shock is further enhancing the unsteady movement within the layer between the separated region and the core flow. The instability is definitely not amplified or even initiated by the expansion waves that result from the reflection of the shock from the opposite wall. Expansion always stabilizes the flow, and this is obviously the case here; the expansion wave system decreases the thickness of the separated region. The pictures in Fig. 20 show another feature of the lambda shock very nicely—the slip line from the Mach triple point. The flow along this line has continuous pressure in direction normal to it, and the velocities on both sides are parallel, but the entropy, density and parallel velocity display a jump across it. Again, in the presence of viscosity, the slip line is a location of a shear layer, destabilizing the flow.

Significantly, the authors in [14] emphasize that even on the symmetry line, the results of numerical flow simulation for the two-dimensional nozzle computed in 2-D and 3-D fashion are vastly different.

The three-dimensional simulations have been performed assuming laminar boundary layers. At the Reynolds-number given (Re=140,000), the flow in a large portion of the nozzle is laminar. The exact location of the transition from laminar to turbulent is not known and is being currently investigated. However, it can be assumed that close to the nozzle exit, the flow will experience transition in view of the massive boundary layer separation due to shock–boundary layer interaction. However, this should not affect the flow structure in forward part of the nozzle. As the authors are aware of this shortcoming (the simulation program CCM+ is not capable of handling partially turbulent flows), the program ACHIEVE is being modified to include transition and partially turbulent flow implementing a non-linear turbulence model.

7. Conclusions

The present work offers one major conclusion; both the low and the high unchoking are the result of unsteady shock–boundary layer interaction, possibly coupled to laminar–turbulent transition. In terms of numerical prediction of the flow field, the present authors see a chance to obtain realistic results in all comprehensive three-dimensional large eddy or even direct simulation. The corresponding computational effort is extremely large due to the required spatial and time-wise resolution.

However, the usefulness of this effort seems somewhat questionable in light of some of the experimental results presented by Mickan et al. in [9]. The resulting mass flow data for the same size, same operational conditions CFVNs of different manufactures displayed very different behavior, the only difference being the inside surface quality of the nozzles.

References

[1] International Standard ISO 9300. Measurement of gas flow by means of critical flow Venturi nozzles. first edition. Berlin: Beuth; 1990.
[2] von Lavante, E, Nath, B and Dietrich, H. Effects of instabilities on flow rates in small sonic nozzles. In: Proceedings of the 9th int. conference on flow measurement FLOMEKO'98, Lund; 1998.
[3] Wendt, G. Ph.D. thesis, University of Essen, Germany; 2000.
[4] Nakao, Shin-ichi. Choking phenomenon of sonic venturi nozzles on low Reynolds numbers. In: Proceedings of the 9th int. conference on flow measurement FLOMEKO'98, Lund; 1998.
[5] von Lavante, E, Ishibashi, M, and Wendt, G. Investigation of flow fields in small sonic venturi.nozzles. In: Proceedings of the 10th int. conference on flow measurement FLOMEKO'2000, Salvador; 2000.
[6] Nakao S-I, Takamoto M. Choking phenomena of sonic nozzles at low Reynolds numbers. FMI 2000;11:314–25.
[7] Nakao, S.-I. High pressure hydrogen gas flow measurements by the critical nozzle flow meter. 3rd Workshop on Critical Nozzles, Quedlingburg, Germany; 2005.
[8] Xiao,Q, Tsai, HM and Papamoschou, D. Numerical Investigationof supersonic nozzle flow separation. AIAA paper 2005-4640.
[9] Mickan, B, Kramer, R and Li, Ch. Critical back pressure ratio in sonic nozzles—the correlation with diffuser geometry and gas composition. In: Proceedings of the 8th ISFFM conference, Colorado, June 20–22; 2012.
[10] von Lavante, E and Grönner, J. Semiimplicit schemes for solving the Navier–Stokes equations. In: Proceedings of the 9th GAMM conference, Lausanne, notes on numerical fluid mechanics, Vieweg; 1992.
[11] Yao, J. Ph.D. thesis, University of Essen, Germany; 1999.
[12] NACA Report 1135, Ames Aeronautical Laboratory, 1953.
[13] Zucker RD. Fundamentals of gas dynamics. Matrix Publishers Inc; 1977.
[14] Deck,Sebastien, Hallard,Remi, and Guillen, Philippe. Numerical Simulations of Steady and Unsteady Separated Nozzle Flows. AIAA Paper 02-0406, 40th Aerospace Sciences Meeting; 2002.